Cell Density Detection Based on a Microfluidic Chip with Two Electrode Pairs

Yongliang Wang
Beijing University of Chemical Technology College of Information Science and Technology
Danni Chen
Beijing University of Chemical Technology College of Information Science and Technology
Xiaoliang Guo (2306402716@qq.com)
Beijing University of Chemical Technology College of Information Science and Technology
https://orcid.org/0000-0001-9072-1554

Research Article

Keywords: Two electrode pairs, Uncertain volume, Cell density, Impedance, Microfluidic.

Posted Date: March 8th, 2022

DOI: https://doi.org/10.21203/rs.3.rs-1237908/v1

Abstract

Cell density detection is usually the counting of cells in certain volume of liquid, which is an important process in the field of biomedicine. The Coulter counting method has been an important method for biological cell detection and counting for decades. In this paper, a microfluidic chip based on two electrode pairs is designed, which uses the Coulter principle to detect the flow rate of uncertain volume liquid and count the cells, and then calculate the cell density by statistics. When the cell passes through the sensor channel formed by the electrode pair on the chip, the impedance will change between the electrodes. This phenomenon has been proved by experiments. The designed chip has the advantages of simple structure, small size and low manufacturing cost. The cell density detection method proposed in this article is of great significance to the research in the field of biological cell detection and development of related medical devices.

1 Introduction

In recent years, the medical field has developed rapidly. In the process of disease detection, it is particularly important to measure the density of cells in the blood[1]. Traditionally, the cell density is obtained manually under a microscope [2–6]. The commonly used statistical method of cell density is to calculate the number of cells in certain volume of liquid[7–10]. This method of cell density detection requires cells to be uniformly distributed in the liquid, and then to count the cells in certain volume of sample[11–14]. Commonly used methods for detecting cells are laser induced fluorescence method[15–19], image processing method[20–26] and electrical impedance method[27–30]. Ivan V Grishagin designed a cell counting program based on image processing, which obtains images of mammalian cell suspension in the hemocytometer component through a conventional optical microscope equipped with a network camera [31]. The corresponding algorithm is designed based on the ImageJ toolbox which can automatically count these cells. Due to the influence of cell aggregation and overlap, the number of cells detected by this method will be relatively low. Byeongyeon Kim et al. designed an rWBC counter based on optical devices (optical imaging sensors) to achieve high-throughput cell counting. The device has a complex structure resulting in the expensive cost to manufacture, and requires specific blood processing before detection[32]. When the biological particles pass through the micropores, the resistance of the pores will increase because the insulating particles replace the conductive solution in the pores. This directly leads to a significant drop in the current passing through the hole, which is commonly referred to as the Coulter principle.

The early IFC chips were based on the principle of Coulter counter using a DC supply. In 2002, Satake developed a silicon-based Coulter counter to detect polystyrene beads and red blood cells (RBCs)[33]. Later, a four-channel parallel micro-Coulter counter was designed to simultaneously detect particles flowing through four sensing channels, and the device was capable of rapidly differentiating and counting micro-polymethacrylate particles and Juniper pollen[34]. To avoid the polarization of metal electrodes, polyelectrolyte salt bridge-based electrodes (PSBEs) have successfully been fabricated using

photopolymerization to distinguish RBCs and white blood cells (WBCs) in human blood[35]. Afterwards, impedance micro-cytometry based on AC supply was established, with microelectrodes integrated into the walls of the microchannel instead of fabricating sensing electrodes at both sides of the aperture. In 2001, Gawad et al. fabricated two pairs of microelectrodes on the bottom of a microchannel and energized them with a voltage at one or more discrete frequencies. One pair is used for sensing the electric current fluctuation caused by a cell, whereas the other acts as a reference. This design can clearly detect the differentiation of beads, erythrocytes, and ghost cells. Following that, a pair of parallel facing electrodes was proposed for impedance sensing and this electrodes design theoretically has a better performance because the electric field distribution is least divergent[36]. Then, a chip with this parallel facing electrodes is fabricated to measure the di-electric properties of ghosts and RBCs[37]. With these two types of electrodes: coplanar and parallel facing electrodes, microfluidic impedance cytometers have been used to analyze a wide variety of particles, human cell lines, phytoplankton, erythrocytes, and bead-labeled CD4 T-lym-phocyte.

Impedance measurement of live biological cells is widely accepted as a label free, non-invasive and quantitative analytical method to assess cell status. This method is easy-to-use and flexible for device design and fabrication. The Coulter counter is a powerful tool for characterizing biological particles suspended in a liquid electrolyte environment[38, 39], and has been widely used in the analysis of particles[40], human cells[41], bacteria[42], viruses[43], DNA and other biological molecules[44, 45].

In this paper, a microfluidic chip with a dual-electrode pair structure is designed based on Coulter principle, which can realize the absolute count of cells in the sample liquid. The single-electrode pair of the chip realizes cell counting, and the double-electrode pair realizes the measurement of cells flow rate. Finally, we calculate the cell density in the detected liquid according to the structure parameters of the chip.

2 Materials And Methods

2.1 Theory and Methods

When single cells pass through a flow system, the electrodes alongside the fluidic channel can detect their impedance signals. When we apply an AC voltage to the electrode pair, the impedance between the electrodes will change because the cell replaces the liquid medium between the electrodes. Since the cell is a kind of insulating particles, when it passes through the electrodes, the impedance change will be significant. By capturing change of the impedance, it is possible to confirm the timing of the cell passing the detection electrode and the number of cells passing the detection electrodes in a period of time. As a non-invasive, label-free electrochemical method, impedance measurements can automatically provide sensitive and quantitative results. These advantages make impedance measurements widely used methods to study cells, especially for live cell analysis and long-time live cell monitoring.

The microfluidic chip in this paper is mainly composed of a dual electrode pair and a microfluidic channel, and there is a micro-sensing channel in the middle of each pair of electrodes. When a cell passes through the micro-sensing channel, the impedance between the electrodes will change significantly. By continuously detecting the impedance signal of the electrode pair, it can detect the change of the impedance signal when certain quantity cells (n) pass, so as to realize the cell count. The distance (s) between the two electrode pairs is fixed. The average flow rate of the cell from one electrode pair to the other one is calculated by detecting the time difference (Δt) of the same cell flowing through the two electrode pairs. The average flow rate of the cell represents the average flow velocity of the liquid in this period of time (v). The width (d) and height (h) of the microchannel are known. The total time from the first cell passing through the first electrode pair to the last cell passing through the second electrode pair is denoted as t. According to the above principle, the cell density can be calculated. The formula for density (ρ) is as follows:

$$\rho = \frac{n}{\bar{v}\,dht}$$

1

The $\bar{v}$ in formula (1) represents the average flow velocity of n cells, and the calculation formula is as follows:

$$\bar{v} = \sum_{i=1}^{n} v_i$$

2

The v_i in formula (2) represents the average flow velocity of each cell between the two electrode pairs, and the calculation formula is as follows:

$$v_i = \frac{s}{\Delta t_i}$$

3

Δt_i in formula (3) represents the time difference between successive cells passing through two electrode pairs.

2.2 Design and fabrication of the chip

The structure diagram of the designed chip is shown as Fig. 1:

The chip utilizes ultraviolet lithography technology to form metal patterns and microchannel patterns on the substrate. The metal pattern is formed on the glass substrate using AZ-5214 (Micro-Chemicals, Ulm, Germany) photoresist. The technological process is shown in Fig. 2(a): (1) After preheating the glass substrate on the heating plate at 110°C for 120 seconds, remove it and cool it to room temperature and

fix it on the turntable of the spin coater;(2) Take 3ml of AZ-5214 photoresist and pour it onto the glass surface. First, spin at 500rpm for 30 seconds with acceleration of 100rpm/ second, and then spin at 1000rpm for 10 seconds with acceleration of 200rpm/second. Let it stand for 5 minutes; (3) Remove the glass substrate, place it on the heating plate and bake it at 110°C for 90 seconds; (4) Expose the glass substrate via a photoetching machine at the exposure energy of 16.7mJ/s•cm2 for 8 seconds; (5) Immerse the exposed glass substrate in the AZ developer (Micro-Chemicals, Ulm, Germany) for 40 seconds; (6) After cleaning the glass substrate with deionized water for 30 seconds, blow it dry with filtered, pressurized nitrogen (do not leave water marks); (7) Post-baking the patterned glass substrate with a 70℃ heating plate for 120 seconds; (8) A layer of Cr (adhesion layer) is first plated on the patterned glass surface with a sputtering apparatus, and then a layer of Au is plated; (9) Soak the metal-plated glass substrate in acetone, and use low-power ultrasonic to wash away the metal on the photoresist other than the metal patterning. Through this process, a metal electrode can be obtained, as shown in Fig. 3(a). Adopt SU-8 2015 photoresist (Micro-Chem Corp, MA, USA) to obtain the convex microchannel pattern on the silicon wafer. The fabrication process is shown in Fig. 2(b). According to the SU-8 2015 user manual, the exposure energy required for lithography of 50um thick pattern is 160mJ/cm2, the exposure energy of the lithography machine is 16.7mJ/s•cm2, and the exposure time is calculated as 9.6 seconds The elastoplastic material polydimethylsiloxane (PDMS) (Sylgard 184, Dow Corning, USA) mixture, with an adequate mix in the ratio of cross-linker/curing agent A: prepolymer B = 1: 10, was degassed and poured onto the SU-8 molds. Then heat it with a 115°C hot plate for 30 minutes to completely cure the PDMS. After separating the PDMS from the silicon wafer, a microchannel structure is formed, which is shown in Fig. 3(b). Place the glass substrate with electrodes in the PLASMA cleaning machine (Harrick, NY, US) for surface treatment, and then fix the glass substrate on the stage of the inverted microscope (Nikon Corp. TI2-U, Japan), so that the microchannel structure on the PDMS can be accurately bonded to the glass sheet with metal electrodes. The complete chip is shown in Fig. 3(c), the actual chip produced is shown in Fig. 3(d), and the chip structure under the microscope is shown in Fig. 3(e).

The structure parameters of the chip are as follows: the distance between the inlet of the chip and the outlet of the chip is 24mm, the width (d) of the main channel is 200um, and the height (h) of the micro-channel is 50um according to the manufacturing process; Micro-sensing channel 1 and micro-sensing channel 2 have the same structural parameters. Their width is 30um, length is 15um, and the center distance (s) between the two electrode pairs is 6mm; The structural parameters of the electrode pair 1 and the electrode pair 2 are the same, the distance between the positive and negative electrodes of the electrode is 1.1 mm, and the center distance between the electrode pair 1 and the electrode pair 2 is 6 mm.

2.3 Experiment setup

The experimental device mainly includes an impedance analyzer (Made in Switzerland), an impedance analysis software (ziControl) on the computer and a microfluidic chip. The schematic diagram of the device configuration is shown in Fig. 4. This type of impedance meter can collect the impedance signals

of two channels at the same time. Through the impedance analysis software, we can obtain the impedance signals of the two electrode pairs (electrode pair 1 and electrode pair 2) on the chip. The software can also store the impedance data of the two channels and time data corresponding to each impedance signal. In order to inject liquid into the microfluidic chip at a steady flow rate, we use a syringe pump to inject the liquid mixed with cells into the chip.

2.4 Cell culture

The experiment used HL60 cells (human promyelocytic leukemia cells), which were cultured in suspension in cell culture medium (1640 + 10% FBS). We place the culture medium for culturing cells in a constant temperature (37°C) incubator while maintaining the pH value of the incubator at 7.2–7.4 and the concentration of CO_2 at 5% and dilute the HL60 cell solution after centrifuging and removing the supernatant according to the requirements of the cell concentration in the experiment.

3 Results And Discussion

3.1 Cells count and flow velocity measurement

Experiments were performed with 20um fluorescent microbeads (Made in Tianjin Base Line Chrom Tech Research Centre) to verify the cell counting efficiency of the chip and the liquid flow rate measurement efficiency. After connecting the experimental device as shown in Fig. 4 above, set the injection speed of the syringe pump to 5ul/min, set the impedance analyzer applying to the two electrode pairs to 1Vpp and the frequency to 500Khz. When the microbeads continuously pass through the two micro-sensing channels, electrode pair 1 and electrode pair 2 generate obvious impedance change signals, as shown in Fig. 5.

When 20um microbeads pass through the micro-sensing channel, they will cause impedance change. The width of the sensing channel will affect the detection results. For this, we make micro-sensing channels with different widths (25um, 30um, 35um, 40um) to optimize the parameter. Set the injection speed of the syringe pump to 5ul/min, set the impedance analyzer applying to the two electrode pairs to 1Vpp and the frequency to 500Kh.The chip parameters are optimized according to the impedance change of the microbeads passing through the micro-sensing channels of different widths. As shown in Fig. 6, the change of impedance decreases as the width of the micro-sensing channel increases. However, when the width of the micro-sensing channel is 25um, the microbeads will block the micro-sensing channel with high probability. Therefore, the micro-sensing channel width of 30um is the best parameter for chip design.

Save the data collected by electrode pair 1 and electrode pair 2, and perform data processing to obtain the impedance value of the two electrode pairs and the time difference (Δt) between the microbeads passing through the two electrodes in turn. By detecting the peak value in the impedance data and the time data corresponding to the peak value, the liquid flow rate (v_i) is obtained according to formula (3).

HL60 cell experiments prove that the cell counting efficiency of the chip and the measurement efficiency of the liquid flow rate are significant. Impedance analyzer parameters remain unchanged and the injection pump speed is set to 5ul/min. When the cell continuously passes through the two micro-sensing channels on the chip, the impedance data and the corresponding time data obtained are shown in Fig. 7.

When the cell passes through the micro-sensing channel, the impedance change of the electrode is smaller than that of the 20um microbead but the signal can be detected. Because the diameter of H160 cells ranges from 5um to 12um, it is generally smaller than the diameter of microbeads.

3.2 Algorithm

For the impedance data of the two channels mentioned above, the peak value of the impedance data and the time corresponding to the peak value are extracted through the multi-peak extraction algorithm, where the number of effective peak values is the number of detected microbeads/cells. The effective peaks are the obvious peaks we can see in the impedance diagram. We hope the computer can find them. Due to the drift of the impedance data, the peak value cannot be extracted directly by setting the threshold of the impedance peak value. Using the well-known zero-derivate method. Due to the noise, which is always there in real-life signals, accidental zero-crossings of the first derivate occur, yielding false detections. The typical solution is to smooth the curve with some low-pass filter, usually killing the original signal at the same time. The result is usually that the algorithm goes horribly wrong where it's so obvious to the eye. But we realize that a peak is the highest point betweem "valleys". What makes a peak is the fact that there are lower points around it. Besides, we require a difference of at least X (a value) between a peak and its surrounding in order to declare it as a peak. Same goes with valleys. This paper uses this strategy to find the highest point: there are points below it on both sides around the highest point. At the same time, the detection time corresponding to the effective peak point is obtained.

As shown in Fig. 8, part of the peak data is extracted from a set of impedance data. Calculate the slope of each point on the curve. According to the change of slope (the slope of peak and valley points is zero), three peak points (P_1, P_2, P_3) and four valley points (V_1, V_2, V_3, V_4) can be identified from the curve. The difference between the effective peak point P_2 and the valley points V_2 and V_3 is much larger than the difference between the noise peak points P_1 and P_3 and the corresponding valley. Therefore, the effective peak point P_2 is extracted as the target peak point, and It can be determined that P_2 is the only peak point in the current data.

3.3 Microbeads experiment results

Through the designed microfluidic chip, as shown in the results of Fig. 9, the number of microbeads can be detected as 10, the detected flow velocity is in the range of 0.006 m/s to 0.011m/s, and the average flow velocity ($\bar{v}$) is 0.0093m/s. The total time (t) for all microbeads to flow through the detection chip is 8.47s. From this, it can be calculated that the average density of microbeads in the liquid is 1.269×10^{10}

beads/ml. The density of the microbeads is 1.40×10^{10} beads/ml. The relative error of the detection results is 9.4%.

3.4 Cell experiment results

Through the designed microfluidic chip, as shown in the results in Fig. 10, the number of cells detected is 11, the flow velocity detected at the same time is in the range of 0.0006m/s to 0.0012m/s, and the average flow velocity ($\bar{v}$) is 0.001m/s. The total time (t) for all microbeads to flow through the detection chip is 40.65 s. From this, it can be calculated that the average cell density in the liquid is 2.71×10^{7} cells/ml. The density of H160 cells was obtained by artificial dilution and sampling and counting under the microscope. The detected cell density was 3.10×10^{7} cells/ml. The relative error of the detected results was 12.6%.

Experiments were carried out using different concentrations of Hl60 cells, and the detection results are shown in the following figure:

3.5 Result analysis

The detection of flow rate through this chip has certain limitations, which is requiring cells to pass through two electrodes in sequence. Once the cells overlap as getting through the electrodes, it will likely lead to missed detection, resulting in lower cell count and flow rate measurement results. However, by comparing the detection signals of microbeads and HL60 cells, it can be seen that when cells of different sizes pass through the electrodes, the impedance peak signals are different. Based on this conclusion, the algorithm can be improved later to solve the problem of missed detection caused by overlapping cells.

The detected cell density and microbead density are lower than the actual density because during the experiment, due to the slow injection speed of the syringe pump, microbeads and cells are easily deposited on the inner wall of the syringe and injection pipe, resulting in the detection result being lower than the actual density.

4 Conclusion

This paper designs a microfluidic chip based on Coulter principle that uses dual electrode pairs to detect cell density. The chip adopts a dual-electrode pair and a micro-sensing channel structure to realize cell counting and liquid flow rate detection, hence obtain the cell density of the liquid to be measured. The microbead experiment and the HL60 cell experiment verified that the method can achieve cell density detection and the relative error of the detection results is within 15%.

The designed microfluidic chip can be used to assist biological cell experiments, helping researchers detect the current density of cultured cells. In addition, it can also be applied to cell counting in biological

blood, and cell density detection. This technology will advance the development of the biomedical field.

Declarations

Acknowledgement

This research was supported by National Natural Science Foundation (61904010), Beijing Natural Science Foundation (4204109), the Central University Fund of China (buctrc201814), the Fundamental Research Funds for the Central Universities (XK1802-4), The Research Fund to the Top Scientific and Technological Innovation Team from Beijing University of Chemical Technology (No. buctylkjcx06).

Data availability

The data that support the findings of this study are available from the corresponding author upon reasonable request.

Disclosures

The authors have no relevant financial interests in the manuscript and no other potential conflicts of interest to disclose.

References

[1] HEJAZIAN M, LI W, NGUYEN N T. Lab on a chip for continuous-flow magnetic cell separation [J]. Lab on A Chip, 2015, 15(4): 959-970.

[2] JIMBO; H C, NGONGO; S I, MBASSI; A, ANDJIGA N G. Novel Quantitative Approach for Predicting mRNA/Protein Counts in Living Cells [J]. Applied Mathematics, 2017, 8): 1128-1139.

[3] MINGHAO Z, LINGUI G, PEIHUA Z, ZHIXIN C, XINQI D. Improvement of cell counting method for Neubauer counting chamber [J]. Journal of clinical laboratory analysis, 2020, 34(1): 23024.

[4] VAN, DE, GEIJN, GERT-JAN, M., VAN, PUL-BOM, NATASJA, BEUNIS, MARLENE. A New Flow Cytometric Method for Differential Cell Counting in Ascitic Fluid [J]. Cytometry, Part B Clinical cytometry: the journal of the International Society for Analytical Cytology, 2016, 90(6): 506-511.

[5] ZENG Y, KE J, JIE L, LIU J, LI S. A low cost and portable smartphone microscopic device for cell counting [J]. Sensors Actuators A Physical, 2018, 274

[6] ZHANG H, DING W, LI S, YA S, QIU B. On-chip analysis of magnetically labeled cells with integrated cell sorting and counting techniques [J]. Talanta, 2020, 220(315): 121351.

[7] ANAS, MOHD, NOOR, TAISUKE, MASUDA, WU, LEI, KOJI, HORIO. A microfluidic chip for capturing, imaging and counting CD3+ T-lymphocytes and CD19+ B-lymphocytes from whole blood [J]. Sensors Actuators B Chemical, 2018.

[8] FREITAS A I, VASCONCELOS C, VILANOVA M, CERCA N. Optimization of an automatic counting system for the quantification of Staphylococcus epidermidis cells in biofilms [J]. Journal of Basic Microbiology, 2014, 54(7):

[9] PUI T S, YU C, WONG C C, NADIPALLI R, RAHMAN A. High density CMOS electrode array for high-throughput and automated cell counting [J]. Sensors Actuators B Chemical, 2013, 181(3): 842-849.

[10] SMADI; O A, AL-MOMANI; T D, ABDALLAT; R G, AWAD S I. Automated identification and counting of proliferating mesenchymal stem cells in bone callus [J]. International Journal of Computational Vision and Robotics, 2019, 9(1): 1-13.

[11] ALAHMARI S S, GOLDGOF D, HALL L, PHOULADY H A, PATEL R H, MOUTON P R. Automated Cell Counts on Tissue Sections by Deep Learning and Unbiased Stereology [J]. Journal of Chemical Neuroanatomy, 2019, 96(94-101).

[12] DRIESCHNER T, OSTERTAG E, BOLDRINI B, LORENZ A, REBNER K. Direct optical detection of cell density and viability of mammalian cells by means of UV/VIS spectroscopy [J]. Analytical Bioanalytical Chemistry, 2020, 412(10):

[13] FALK T, MAI D, BENSCH R, ÇIçEK Ö, ABDULKADIR A, MARRAKCHI Y, BöHM A, DEUBNER J, JäCKEL Z, SEIWALD K. U-Net: deep learning for cell counting, detection, and morphometry [J]. Nature Methods, 2019.

[14] TIAN Y, CHEN X, LIANG Z, LI D, XIONG Y, XIONG P, GUAN Y, HOU S, HU Y, CHEN S. Microfluidic dielectrophoresis device for trapping, counting and detecting Shewanella oneidensis at the cell level [J]. Biosensors Bioelectronics, 2018, 99(416).

[15] C.; P, S.; S, M.; G R O, F. N. Fluorescence based cell counting in collagen monolayer cultures of primary hepatocytes [J]. Cytotechnology, 2016, 68(4): 1647-1653.

[16] GAMARRA; M, ZUREK; E, ESCALANTE; H J, HURTADO; L, SAN-JUAN-VERGARA. H. Split and merge watershed: A two-step method for cell segmentation in fluorescence microscopy images [J]. Biomedical Signal Processing and Control, 2019, 53(101575).

[17] QI Y, LU X, FENG Q, FAN W, LIU C. An Enzyme-Free MicroRNA Assay Based on Fluorescence Counting of Click Chemical Ligation-Illuminated Magnetic Nanoparticles with Total Internal Reflection Fluorescence Microscopy [J]. ACS Sensors, 2018, 3(12): 2667-2674.

[18] RICCIO D, BRANCATI N, FRUCCI M, GRAGNANIELLO D. A New Unsupervised Approach for Segmenting and Counting Cells in High-Throughput Microscopy Image Sets [J]. IEEE Journal of Biomedical and Health Informatics, 2019, 23(1): 437-448.

[19] TAMMINGA G G, PAULITSCH-FUCHS A H, JANSEN G J, EUVERINK G. Different binarization processes validated against manual counts of fluorescent bacterial cells [J]. Microbiol Methods, 2016, 128(118-124.

[20] IMASHIRO; C, TOKUOKA; Y, KIKUHARA; K, YAMADA; T G, TAKEMURA; K, FUNAHASHI A. Direct Cell Counting Using Macro-Scale Smartphone Images of Cell Aggregates [J]. IEEE Access, 2020, 8(170033-170043.

[21] HE S, MINN K T, SOLNICA-KREZEL L, ANASTASIO M A, LI H. Deeply-supervised density regression for automatic cell counting in microscopy images [J]. Medical Image Analysis, 2021, 68(9): 101892.

[22] YANG B, CHEN B, HE M, YIN X, XU C, HU B. Aptamer-Based Dual-Functional Probe for Rapid and Specific Counting and Imaging of MCF-7 Cells. [J]. Analytical Chemistry, 2018, 90(3): 2355-2361.

[23] MOHD SAFUAN S N, MD TOMARI M R, WAN ZAKARIA W N. White blood cell (WBC) counting analysis in blood smear images using various color segmentation methods [J]. Measurement Science & Technology, 2018, 116(543-555).

[24] COAKLEY; A, ORLOWSKI; T J, MUHLBAUER; A, MOY; L, SPEISER J J. A comparison of imaging software and conventional cell counting in determining melanocyte density in photodamaged control sample and melanoma in situ biopsies [J]. Journal of Cutaneous Pathology, 2020, 47(8): 675-680.

[25] AHN D, ;LEE J, PARK T, MOON S. Human-level blood cell counting on lens-free shadow images exploiting deep neural networks [J]. Analyst, 2018, 143(22): 5380-5387.

[26] TRAN M V, SUSUMU K, MEDINTZ I L, ALGAR W R. Supraparticle Assemblies of Magnetic Nanoparticles and Quantum Dots for Selective Cell Isolation and Counting on a Smartphone-Based Imaging Platform [J]. Analytical Chemistry, 2019, 91(18): 11963-11971.

[27] CASELLI; F, NINNO; A D, BUSINARO; R R L, BISEGNA P. A Bayesian Approach for Coincidence Resolution in Microfluidic Impedance Cytometry [J]. IEEE Transactions on Biomedical Engineering, 2021, 68(1): 340-349.

[28] HASSAN U, WATKINS N N, EDWARDS C, BASHIR R. Flow metering characterization within an electrical cell counting microfluidic device [J]. Lab on a chip, 2014, 14(8): 1469-1476.

[29] SOBAHIA; N, HANBCD A. High-throughput and label-free multi-outlet cell counting using a single pair of impedance electrodes [J]. Biosensors & bioelectronics, 2020, 166(112458).

[30] MANSOORIFAR A, KOKLU A, BESKOK. A. Quantification of Cell Death Using an Impedance-Based Microfluidic Device [J]. Analytical chemistry, 2019, 91(6): 4140-4148.

[31] GRISHAGIN I V. Automatic cell counting with ImageJ [J]. Analytical biochemistry, 2015, 473(63-65.

[32] KIM B, SHIN S, LEE Y, UM C, YOU D, UN H, CHOI S. High-throughput residual white blood cell counter enabled by microfluidic cell enrichment and reagent-containing patch integration [J]. Sensors & Actuators B: Chemical, 2019, 283(549-555).

[33] DAISUKE SATAKE, HIROYUKI EBI, NARIHIRO OKU, KOICHIRO MATSUDA, HIDEKUNI TAKAO, MITSUAKI ASHIKI, ISHIDA M. A sensor for blood cell counter using MEMS technology [J]. Sensors and Actuators B: Chemical, 2002, 83(1-3): 77-81.

[34] JAGTIANI A V, ZHE J. A multiplexed microfluidic impedance sensor for high throughput analysis of microparticles; proceedings of the 2011 16th International Solid-State Sensors, Actuators and Microsystems Conference, F, 2011 [C].

[35] KIM C T C H. Cytometry and velocimetry on a microfluidic chip using polyelectrolytic salt bridges [J]. Analytical Chemistry, 2005, 77(8): 2490-2495.

[36] MORGAN T S N G G S G H. Analytical electric field and sensitivity analysis for two microfluidic impedance cytometer designs [J]. IET Nanobiotech, 2007, 1(5): 69-79.

[37] CHUN T D C, HEE CHAN KIM. Cytometry and Velocimetry on a Microfluidic Chip Using Polyelectrolytic Salt Bridges [J]. Anal Chem, 2005, 77(8): 2490-2495.

[38] ASGHAR; W, WAN; Y, ILYAS A. Electrical fingerprinting, 3D profiling and detection of tumor cells with solid-state micropores [J]. Lab on a Chip, 2012, 12(13): 9.

[39] GUO J, PUI T, RAHMAN A, KANG Y. 3D numerical simulation of a Coulter counter array with analysis of electrokinetic forces [J]. ELECTROPHORESIS, 2013, 34(3): 417-424.

[40] JAGTIANI A V A, ZHE J A, HU J B, CARLETTA J C. Detection and counting of micro-scale particles and pollen using a multi-aperture Coulter counter [J]. Measurement Science and Technology, 2006, 17(1706-1714.

[41] WU; Y, HAN; X, BENSON; J D, ALMASRI; M. Erratum to: Micromachined Coulter counter for dynamic impedance study of time sensitive cells [J]. Biomedical Microdevices, 2013, 15(2): 381.

[42] ZHENG S, NANDRA M S, TAI Y C. Human Blood Cell Sensing with Platinum Black Electroplated Impedance Sensor; proceedings of the Nano/Micro Engineered and Molecular Systems, 2007 NEMS '07 2nd IEEE International Conference on, F, 2007 [C].

[43] ZWICKER J I. Impedance-based flow cytometry for the measurement of microparticles [J]. Seminars in thrombosis and hemostasis, 2010, 36(8): 819-823.

[44] BAYLEY; H, MARTIN C R. Resistive-pulse sensing - From microbes to molecules [J]. Chemical Reviews, 2000, 100(7): 2575-2594.

[45] STEINBOCK; L J, OTTO; O, CHIMEREL; C, GORNALL; J, KEYSER U F. Detecting DNA Folding with Nanocapillaries [J]. Nano Letters, 2010, 10(7): 2493-2497.

Figures

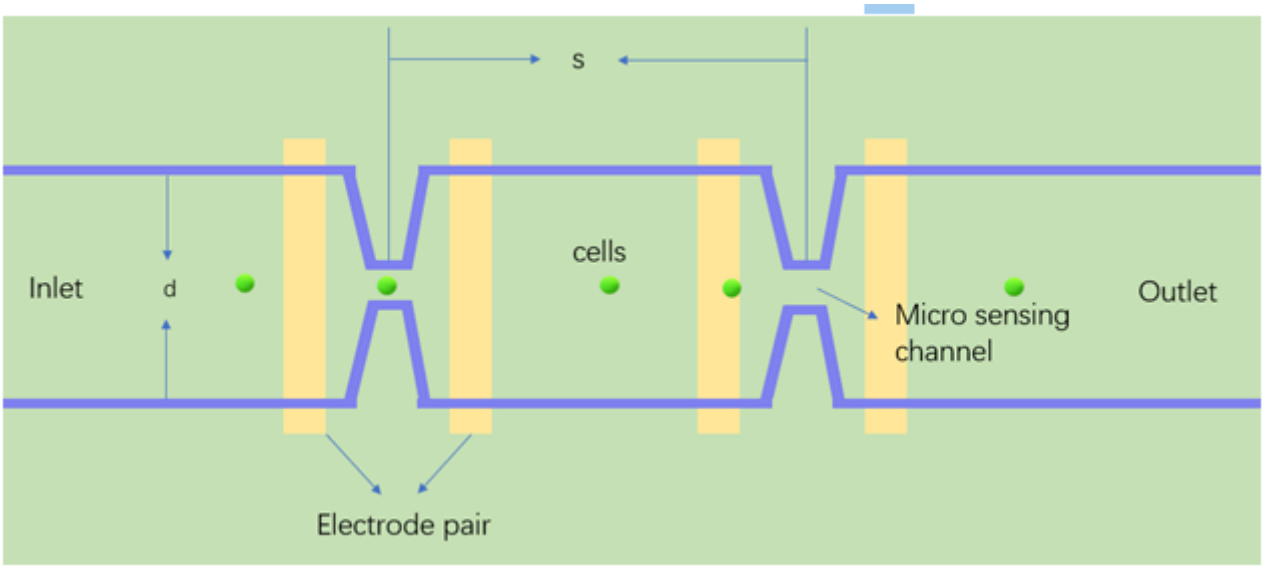

Figure 1

Schematic diagram of chip structure

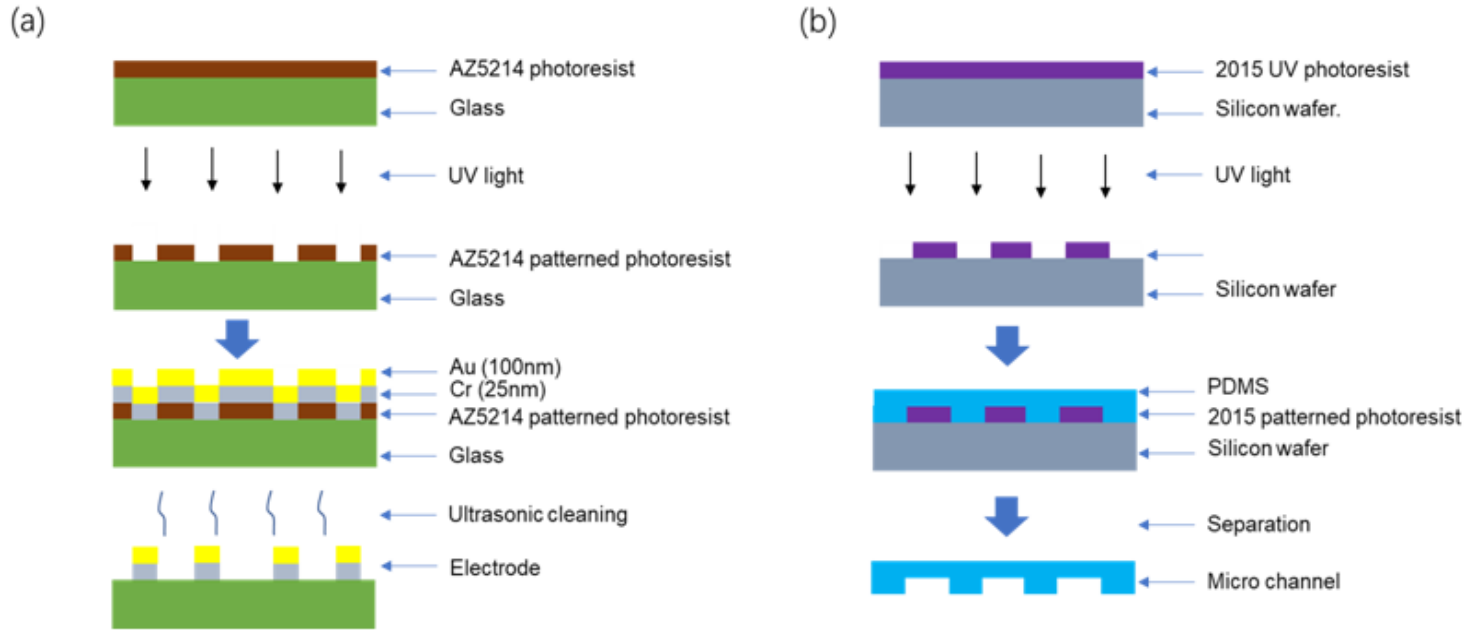

Figure 2

The chip process flow chart: (a) Electrode pair manufacturing process; (b) Micro flow channel manufacturing process.

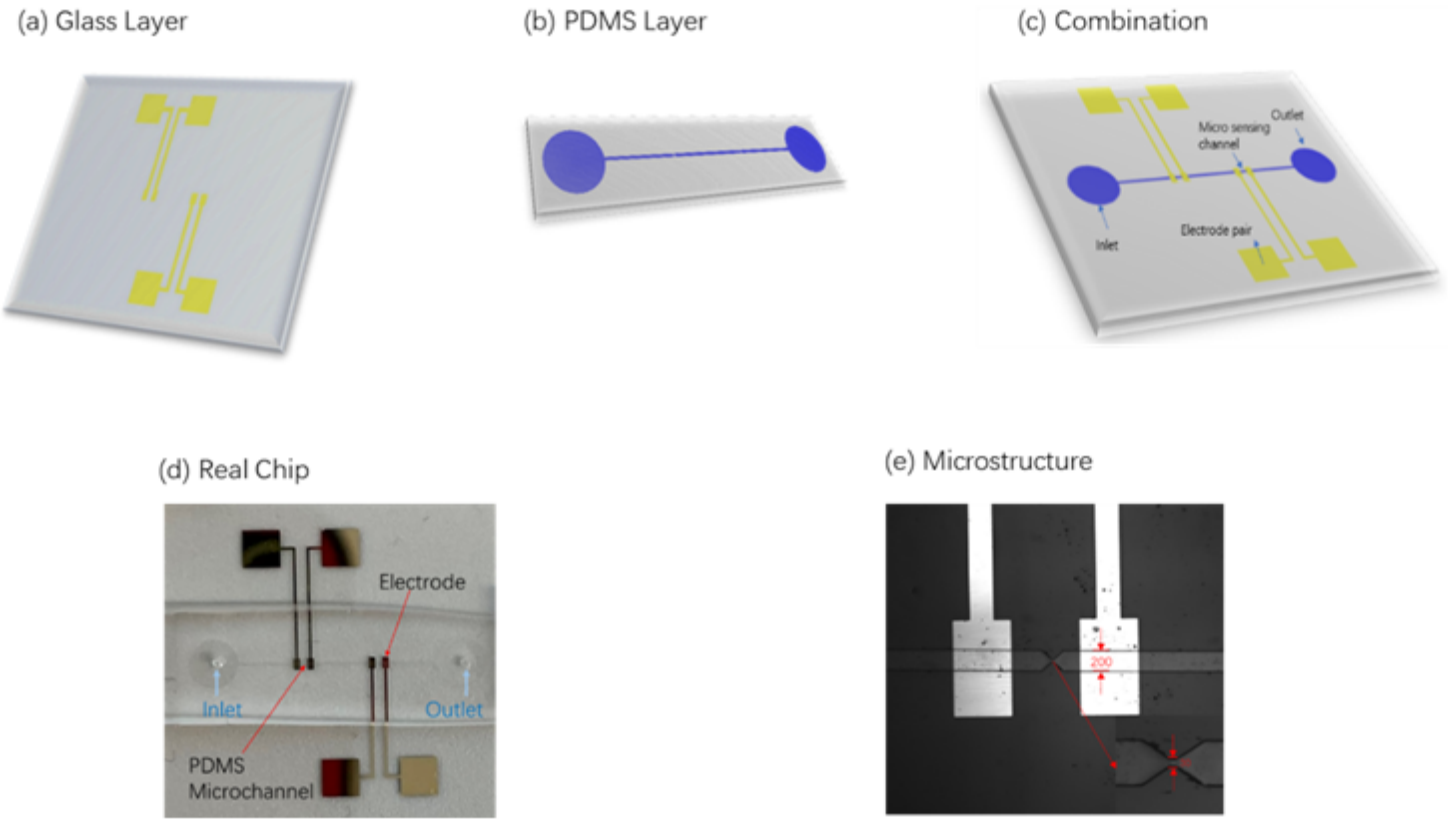

Figure 3

Cell density statistics chip process diagram: (a) glass layer with metal electrode pair; (b) PDMS layer with micro sensor channel; (c) bonding diagram of PDMS and metal electrode pair; (d) physical image of chip; (e) The structure diagram under the microscope of the chip.

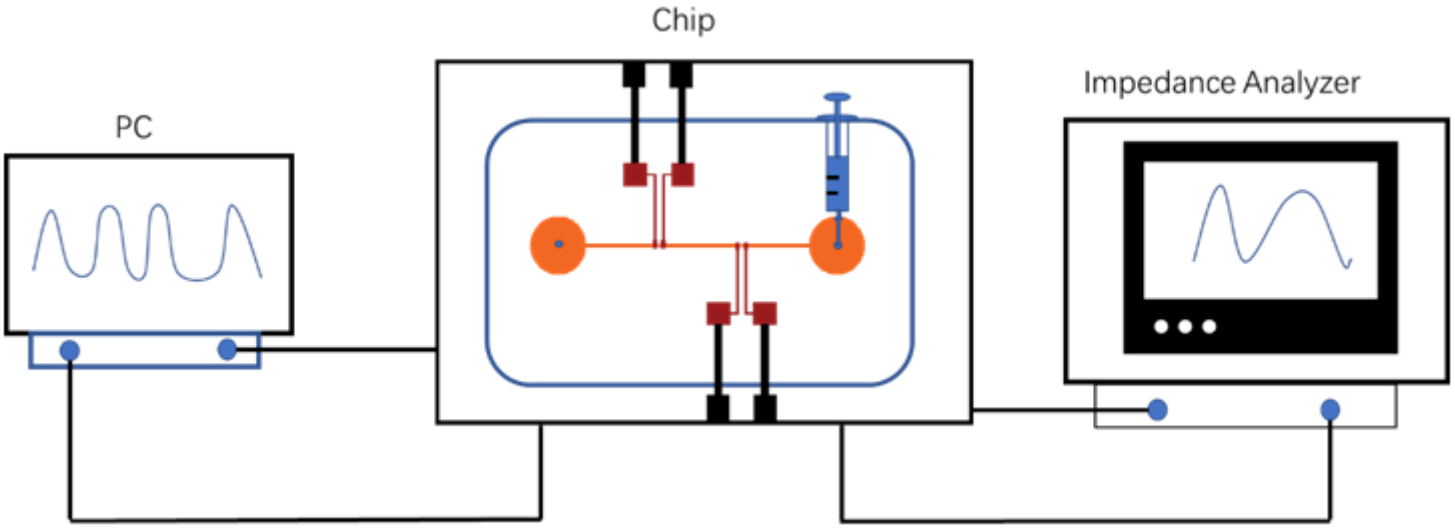

Figure 4

Configuration diagram of testing equipment

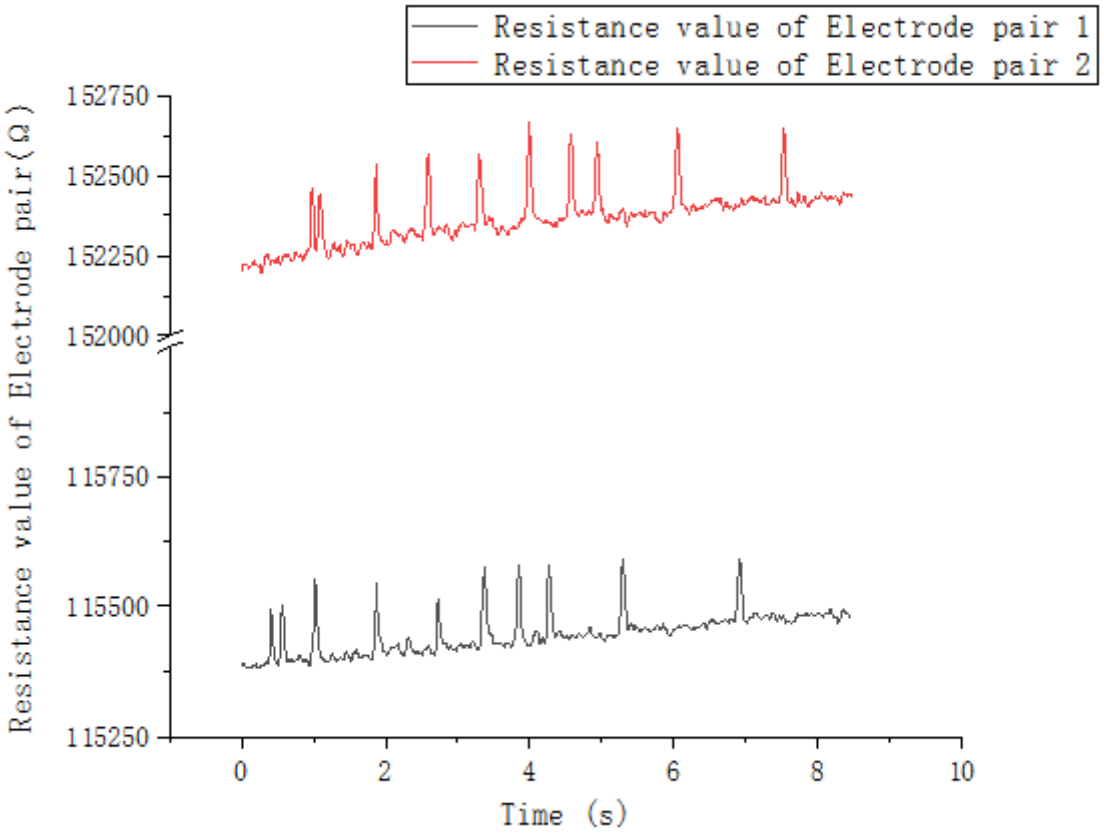

Figure 5

Microbead impedance signal detection diagram

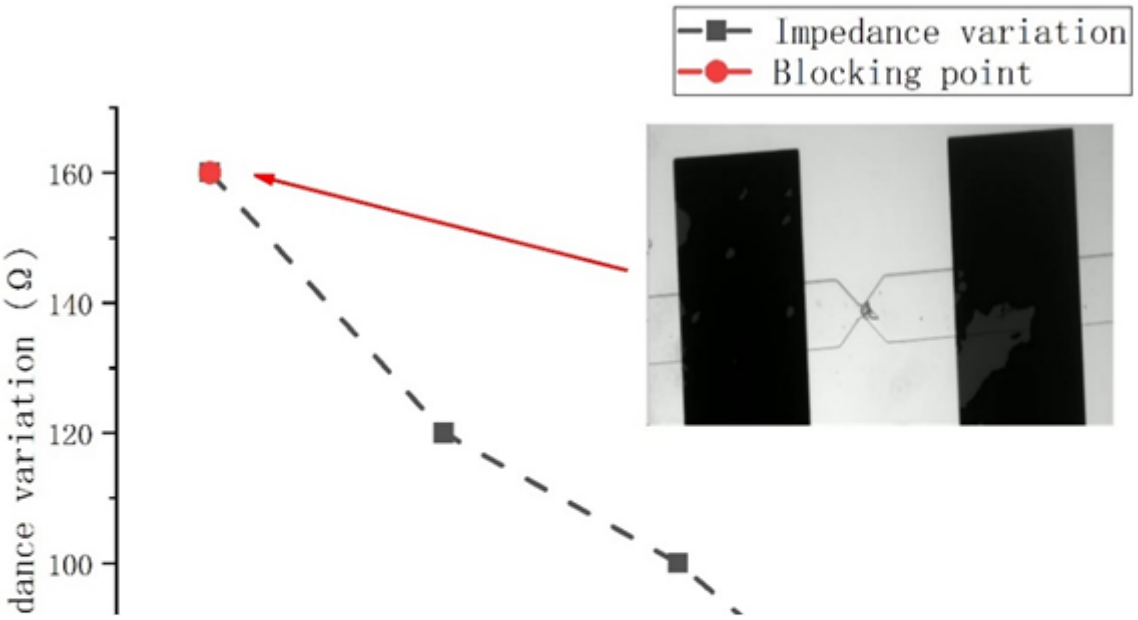

Figure 6

the optimization analysis of the chip micro-sensing channel width

Figure 7

HL60 impedance signal detection diagram

Figure 8

the multi-peak extraction algorithm

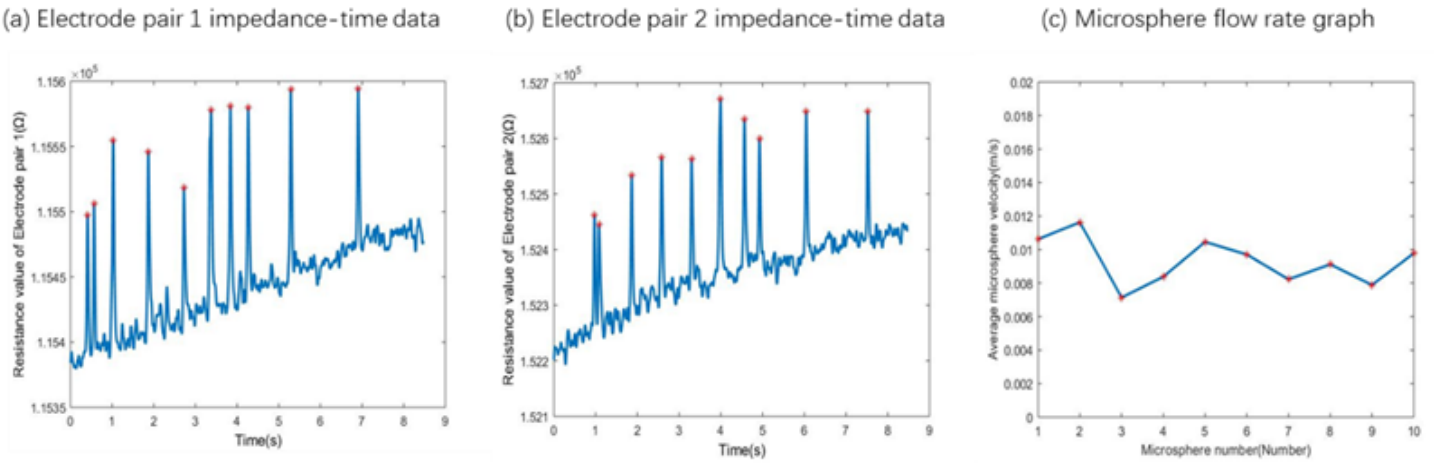

Figure 9

Experimental results of microbeads: (a) Impedance peak extraction of electrode 1; (b) Impedance peak extraction of electrode 2; (c) Flow velocity of microbeads

Figure 10

Experimental results of microbeads: (a) Impedance peak extraction of electrode 1; (b) Impedance peak extraction of electrode 2; (c) Flow velocity of cells

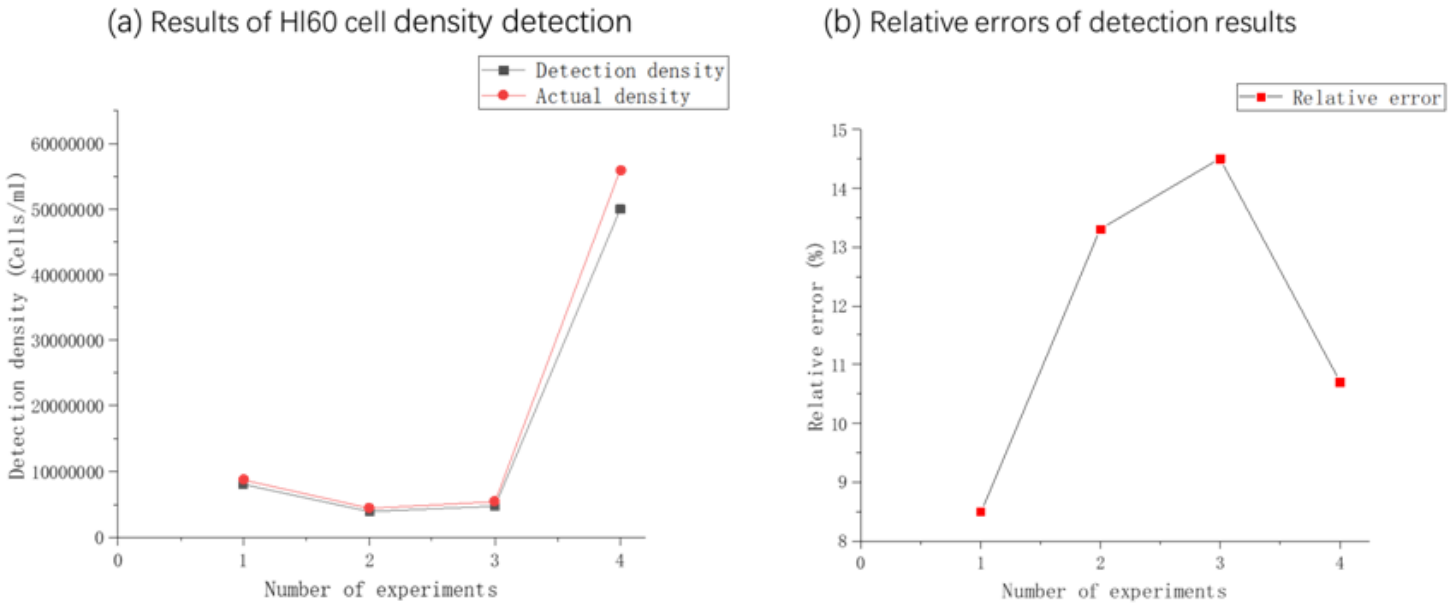

Figure 11

The detection results of Hl60 cells at different densities:(a)Hl60 cell density detection results ;(b)Relative errors of detection results